A Computational Model for Thin Film Formation during Ion Beam Mixing†

Qiang PANG*, Yasuo TAKAHASHI** and Katsunori INOUE***

Abstract

A computational model for thin film formation during ion beam mixing is described in detail on the basis of the binary collision approximation (BCA). A new approach for the effect of residual gas on the growing thin film is also presented. This model has been applied for simulating AlN thin film formation under the condition of nitrogen ion energies of 0.25~1.5keV and Al/N transport ratios of 0.5~2.0. The calculated results show that ion energy plays an important role on the composition of the bulk film and the formation of the interface between the film and the substrate. The calculated results are also compared with experimental ones to demonstrate the abilities of the model. A fine agreement is shown for the transport ratio Al/N≥1. On the other hand, a discrepancy exists in the range of the transport ratio Al/N<1, the reason for which is discussed.

KEY WORDS: (Thin film) (Ion beam mixing) (BCA) (Monte Carlo Method) (Computer simulation) (Aluminum nitride)

1. Introduction

Ion beam mixing (vapor deposition plus simultaneous ion implantation) techniques have been of growing interest in thin film research and application owing to their flexible control of thin film composition and properties. In general, the composition and structure of thin films formed during ion beam mixing are determined by a complex interplay of collisional and chemical effects. It is widely accepted that ions may act physically through collisional effects such as implantation, sputtering or recoil implantation, and they may also promote chemical reactions, or enhance thermal diffusion at both the surface and the inside of a thin film.

Insufficient knowledge about the mechanisms of these effects makes it difficult to create a complete model for the formation of thin films during ion beam mixing. Nevertheless, if chemical effects are neglected and only pure collisional effects are taken into account, the growth and composition changes of thin films may be described as resulting from vapor deposition plus the collisional effects of ion implantation. In such a case, it becomes possible to build a model for the growth of thin films. The calculated results can help us to understand the dynamic composition changes of thin films caused by pure collisional effects. Moreover, in comparison with the experimental results, they can indicate whether other mechanisms are important.

Several analytical models [1,2] have been suggested to describe the growth of thin films. But each of these models requires a number of restrictions and simplifications. It is also difficult to apply them when short of basic data on collisional effects, such as sputtering yields, reflected yields and depth distribution of implanted ions. On the other hand, Monte Carlo computer simulations based on the binary collision approximation have been effective in obtaining data relative to collisional effects [3-7]. The simulation code-TRIM [3-5] and its updated code-TRIDYN [6,7] have been widely accepted and applied for studies of ion implantation, sputtering and atomic mixing. The latter can adjust the target composition dynamically. Therefore it is a better way to modify dynamic simulation codes for representing the growth of thin films during ion beam mixing. Several examples of such works have been given elsewhere [8-11]. With the use of modified TRIDYN, Möller [8] and Bouchier [11] have performed simulations of boron nitride film formation on Ag substrate during ion beam mixing.

In the present paper, a simplified model based on the

† Received on May 19, 1997
* Graduate Student, Osaka University
** Associate Professor
*** Professor

Transactions of JWRI is published by Joining and Welding Reseach Institute of Osaka University, Ibaraki, Osaka 567, Japan.

BCA for the growth of thin films during ion beam mixing and its computer simulation algorithm will be given in detail. The simulations of aluminium nitride (AlN) film formation on a silica (SiO_2) substrate are performed under different nitrogen ion energies and transport ratios of Al/N (the ratio of Al and N atoms arriving at the substrate per unit time) . On the basis of such calculations, the effects of nitrogen ion energy and the transport ratio of Al/N on the formation of the films will be discussed. In addition, for the effect of residual gas (oxygen) on the formation of AlN films, a new approach will be also described. Several examples of computer simulations will be compared with experiments to demonstrate the abilities of this model.

2. The computational model

2.1 Modelling the growth of thin films during ion beam mixing

It is known that the formation of thin films during ion beam mixing is a complex process. Even when considering collisional effects only, some assumptions are necessary to build a model to represent the formation of thin films. The main assumptions in the present model are described as following. The actual ion beam mixing process in a minimal time is assumed to be replaced by two independent and successive processes(vapor deposition and ion implantation) for the convenience of the calculation. The adsorption yield is assumed as 1.0 for each of evaporated atoms. The substrate and the deposition layers are assumed to be amorphous substances since the BCA is used to simulate ions' transport. The composition of the substrate and the deposition layer is assumed to be determined by pure collisional effects. Because local expansions or contractions must be caused inside the substrate, while the defects such as vacancies and interstitial atoms are generated from ion implantation, the substrate relaxation should be taken into account. It is assumed to be realized in minimal time by means of adjusting the local densities in terms of the local composition.

According to the above assumptions, the growth of thin film is illustrated in **Fig.1**. The differential flux ΔD (about 10^{13} atoms/cm^2) is defined as the number of evaporated atoms and ions arriving at the surface of the substrate within a minimal differential time Δt. The corresponding differential flux ΔD_{atom} of evaporated atoms or differential flux ΔD_{ion} of ions is determined by the transport ratio R_f and the given ΔD. As shown in **(a)**, the surface region of the semi-infinite substrate is initially subdivided into M thin slabs of equal thickness which is chosen to be close to that of one monatomic

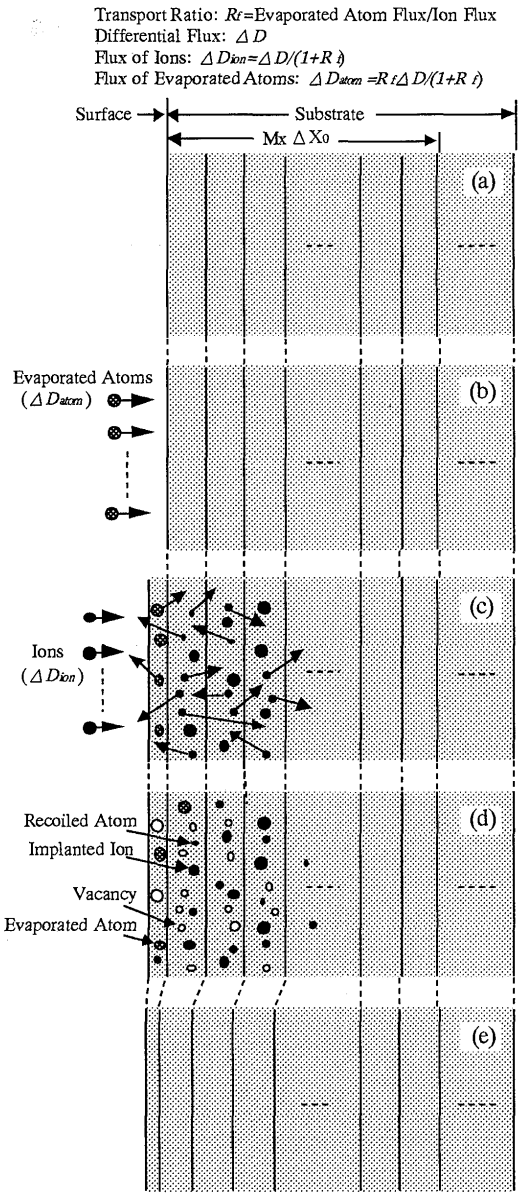

Fig.1 Schematic illustration of the growth of thin film and substrate relaxation. Thin film is assumed to grow up stepwise as the procedures from (b) to (e) are repeated.

layer of the substrate (2~3Å) according to Möller [11]. The evaporated atoms with a flux of ΔD_{atom} are deposited at the surface of the substrate as seen in **(b)**. Ions with a flux of ΔD_{ion} are bombarded on the substrate in **(c)**. After this stage, defects such as vacancies and additional atoms are generated inside the substrate, which is shown in **(d)**. Due to these defects, the substrate relaxation occurs to adjust the thickness of the slabs as seen in **(e)**. These steps (b) to (e) are produced only in a differential time, i.e., thin film is assumed to grow up through the iterative

steps from (b) to (e).

The computational procedure involves three parts, i.e., the evaporated atom deposition, the ion implantation, and the substrate relaxation. For the evaporated atom deposition (step(a) in Fig.1), the evaporated atoms are adsorbed on the first thin slab of the substrate to form a thin layer because their energies are very low and can be neglected in comparison with any initial ion energy. On the other hand, for the ion implantation, the Monte Carlo Method based on the BCA is employed to simulate transport of thousands of ions and the cascades to obtain necessary data such as depth distribution of implanted ions, sputtering yield and atomic mixing. For the substrate relaxation, the thickness of each slab is adjusted according to the change of its local atomic density.

The basic principles and main computational equations used in the present model are given below in detail on the basis of the references [3-7].

2.2 Basic principles and computational equations

2.2.1 Transport of energetic atoms in a solid

In the binary collision approximation, the movement of any energetic atom (ion or recoiled atom) in a target substance is described by sequential elastic collisions with the target atoms. The energy losses of the energetic atom result from both elastic and inelastic collisions, and the movement direction is changed by elastic collisions. The path of an incident ion in a solid is shown partly in **Fig.2**. The ion moves into the solid along its incident direction. After a straight free flight, it will collide with a target atom, and then lose part of its energy and change its direction. The ion will then move with its new direction until it collides with another target atom. Such elastic collisions will occur repeatedly until the ion has lost its energy or escaped from the solid. The species and the position of a target atom for each elastic collision are

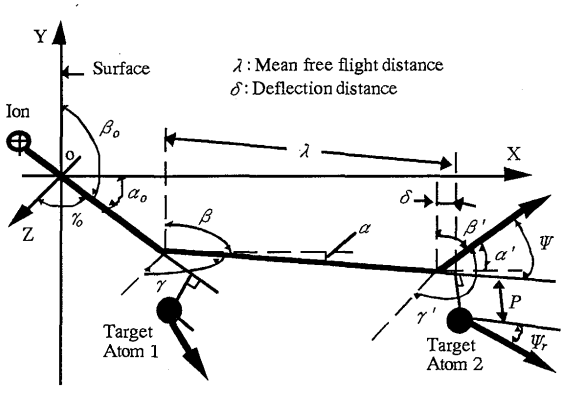

Fig.2 Path of an incident ion and sequential elastic collisions with target atoms in a solid.

determined randomly.

Except for the first collision(described in *2.2.4*), a straight mean free path between two sequential collisions is determined by the local atomic density of the substrate, and its length λ is given by

$$\lambda = n^{-1/3} \tag{1}$$

where n is the local atomic density of the substrate. If the locus of an atom is given by its position (x,y,z) and its directional angles α,β and γ in a fixed Cartesian system immediately after a collision, then the position (x',y',z') after the subsequent collision is given by

$$\begin{aligned} x' &= x + (\lambda - \delta)\cos\alpha, \\ y' &= y + (\lambda - \delta)\cos\beta, \\ z' &= z + (\lambda - \delta)\cos\gamma \end{aligned} \tag{2}$$

where δ denotes the distance of the asymptotic deflection point from the plane which is determined by the original position of the target atom and described below. If a scattering angle ψ and an azimuthal angle ϕ (as shown in **Fig.3**) are used to describe each collision, then the new direction of the energetic atom is obtained by

$$\begin{aligned} \cos\alpha' &= \cos\psi\cos\alpha + \sin\psi\cos\phi\sin\alpha, \\ \cos\beta' &= \cos\psi\cos\beta - \frac{\sin\psi}{\sin\alpha}(\cos\phi\cos\alpha\cos\beta - \sin\phi\cos\gamma), \\ \cos\gamma' &= \cos\psi\cos\gamma - \frac{\sin\psi}{\sin\alpha}(\cos\phi\cos\alpha\cos\gamma + \sin\phi\cos\beta), \end{aligned} \quad \cdots\cdots \tag{3}$$

and its new energy is given by

$$E' = E - \Delta E_{nucl} - \Delta E_{nlel} - \Delta E_{lel} \tag{4}$$

where E is the kinetic energy of the energetic atom before the collision, and ΔE_{nucl}, ΔE_{nlel} and ΔE_{lel} are the elastic energy loss, nonlocal electronic energy loss and local electronic energy loss, respectively. Any of these energy losses is caused by the elastic collision or the inelastic collision, and is described below in detail.

2.2.2 Elastic collisions

The elastic collision occurs between the two nuclei of an energetic atom and a target atom. After collision, the energetic atom not only transfers part of its energy to the target atom but also changes its direction.

As shown in Fig.3, the target atom within a disc of radius P_{max} is chosen for each collision. We assume that only one collision occurs in the volume with a cylinder of length λ and radius P_{max}. At that stage, the radius P_{max} can be represented as

$$P_{max} = (\lambda\pi n)^{-1/2}. \tag{5}$$

The actual impact parameter P is determined randomly according to

$$P = P_{max}\sqrt{r_1} \tag{6}$$

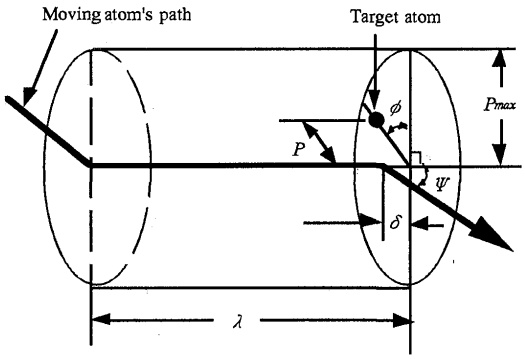

Fig.3 Definition of the target atom position, determined by the impact parameter P and azimuthal angle ϕ.

where r_1 is a random number between 0 and 1. In our present model, any random number is generated by calling up a random function in the computer. The azimuthal angle of the target atom ϕ is given by

$$\phi = 2\pi r_2 \tag{7}$$

where r_2 is a random number between 0 and 1. The species j of the target atom is determined randomly from the local composition according to

$$j = \min(k: \sum_{i=1}^{k} f_i \geq r_3) \tag{8}$$

where r_3 is a random number between 0 and 1, and f_i is the concentration of atomic species i.

Fig.4 illustrates schematically, elastic collisions between two atoms in different reference systems (a) and (b). The relation of the scattering angles between the two systems is given by

$$\tan\psi = \frac{\sin\theta}{m_1/m_2 + \cos\theta}, \tag{9}$$

and

$$\tan\psi_r = \frac{\sin\theta}{1-\cos\theta}. \tag{10}$$

A screened Coulomb interatomic potential

$$V(r) = \frac{Z_1 Z_2 e^2}{4\pi\varepsilon_0 r}\Phi\left(\frac{r}{a}\right) \tag{11}$$

with the 'Kr-C' screening function [16]

$$\Phi(\omega) = 0.191e^{-0.279\omega} + 0.474e^{-0.637\omega} + 0.335e^{-1.919\omega} \tag{12}$$

is chosen as the interatomic potential. In formula (11), Z_1 and Z_2 denote the charges of the scattered atom and target atom, e the charges of one electron, ε_0 the electric inductivity, r the distance between two atoms, and a the Firsov's screening distance which is given by

$$a = \frac{0.8853 a_0}{(Z_1^{1/2} + Z_2^{1/2})^{2/3}} \tag{13}$$

with the radius of the first orbit, $a_0 = 0.0529\,\text{nm}$. The closest distance r_c between two atoms is determined from

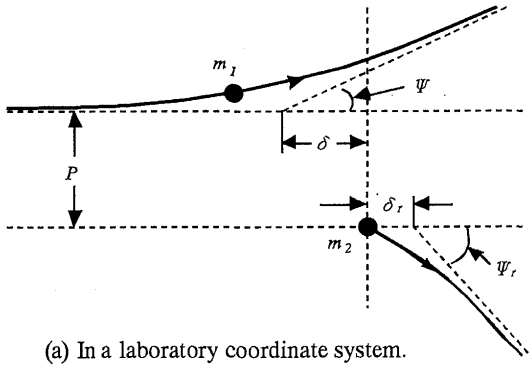

(a) In a laboratory coordinate system.

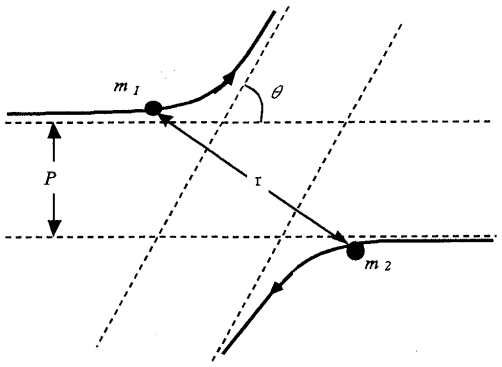

(b) In a center of mass coordinate system.

Fig.4 The elastic collision diagram of two particles in different reference systems.

$$1 - \frac{V(r_c)}{E_C} - \left(\frac{P}{r_c}\right) = 0 \tag{14}$$

with the center of mass energy

$$E_C = \frac{m_2}{m_1 + m_2}E \tag{15}$$

where m_1 and m_2 denote the atomic masses of the scattered atom and the target atom. Equation (14) can be solved by Newton's method. After obtaining the value of r_c, the scattering angle θ in the center of mass system can be calculated according to

$$\theta = \pi - 2P\int_{r_c}^{\infty}\left[1 - \frac{V(r)}{E_C} - \left(\frac{P}{r}\right)^2\right]\frac{dr}{r^2}. \tag{16}$$

The offset of deflection point is calculated in an hard sphere approximation according to

$$\delta = r_c \sin\frac{\theta}{2}. \tag{17}$$

The elastic energy loss, i.e. the energy transferred to the target atom, is given by

$$\Delta E_{nucl} = \frac{4m_1 m_2 E}{(m_1 + m_2)^2}\sin^2\frac{\theta}{2}. \tag{18}$$

2.2.3 Inelastic collisions

The inelastic collisions are defined as the collisions between the energetic atom's nucleus and the target atom's

electrons. Due to an electronic mass much less than that of a nucleus, any inelastic collision has been assumed not to change the moving direction of the energetic atom.

At low ion energies ($E \leq 25KeV/amu$), Lindhard and Scharff's formula[17]

$$S_e = \frac{1.212 Z_1^{7/6} Z_2}{(Z_1^{2/3}+Z_2^{2/3})^{3/2}} \sqrt{\frac{E}{m_1}} \ (eV Å^2) \qquad (19)$$

is used for the calculation of the electronic stopping cross section. So the nonlocal inelastic energy loss is given by

$$\Delta E_{nlel} = (\lambda - \delta) n S_e \ , \qquad (20)$$

and the local inelastic energy loss is given by

$$\Delta E_{lel} = \frac{0.045 S_e}{\pi a^2} e^{-0.3 r_c / a} \qquad (21)$$

according to Oen and Robinson [18].

2.2.4 *Initial conditions of incident ions and recoil atoms*

The X axis of a fixed Cartesian system is chosen to be perpendicular to the substrate surface. For the given incident angle α_0 (the angle of incident direction and X axis) and initial energy E_0, an incident ion is assumed to start to move towards the substrate according to the directional angles determined by

$$\begin{aligned} \cos\alpha_0 &= \cos\alpha_0, \\ \cos\beta_0 &= \sin\alpha_0 \cos(2\pi r_4), \\ \cos\gamma_0 &= \sin\alpha_0 \sin(2\pi r_4) \end{aligned} \qquad (22)$$

with a random number r_4 between 0 and 1 if the substrate rotates upon the X axis during ion implantation. If the substrate surface is assumed to be rough on the scale of a monatomic layer, and the starting position is given by $(x_{surf}, 0, 0)$ where x_{surf} is the position of the substrate surface, then the first position of collision is determined by

$$\begin{aligned} x_1 &= x_{surf} + \lambda r_5 \cos\alpha_0, \\ y_1 &= \lambda r_5 \cos\beta_0, \\ z_1 &= \lambda r_5 \cos\gamma_0 \end{aligned} \qquad (23)$$

where r_5 is a random number between 0 and 1.

After an elastic collision, a new recoil may be caused if the elastic energy transfer is larger than the bulk binding energy $E_{b,j}$. Its start energy is given by

$$E_{r0} = \Delta E_{nucl} - E_{b,j} \ , \qquad (24)$$

its start position by

$$\begin{aligned} x_r &= x + \lambda\cos\alpha - P\cos\phi\sin\alpha, \\ y_r &= y + \lambda\cos\beta + \frac{p}{\sin\alpha}(\cos\phi\cos\alpha\cos\beta - \sin\phi\cos\gamma), \\ z_r &= z + \lambda\cos\gamma + \frac{P}{\sin\alpha}(\cos\phi\cos\alpha\cos\gamma + \sin\phi\cos\beta) \end{aligned} \qquad \ldots\ldots (25)$$

where x, y and z are equivalent to those described in 2.2.1 , and its direction by

$$\begin{aligned} \cos\alpha_r &= \cos\psi_r\cos\alpha - \sin\psi_r\cos\phi\sin\alpha, \\ \cos\beta_r &= \cos\psi_r\cos\beta + \frac{\sin\psi_r}{\sin\alpha}(\cos\phi\cos\alpha\cos\beta - \sin\phi\cos\gamma), \\ \cos\gamma_r &= \cos\psi_r\cos\gamma + \frac{\sin\psi_r}{\sin\alpha}(\cos\phi\cos\alpha\cos\gamma + \sin\phi\cos\beta). \end{aligned} \qquad \ldots\ldots (26)$$

2.2.5 *Stopping conditions of moving ions and recoil atoms*

An incident ion or a recoil atom is judged to stop its movement when it has been slowed down to an energy below a given cutoff energy inside the substrate, or it has moved outside the substrate with the normal fraction of its energy larger than its surface binding energy $E_{sbe,i}$, i.e.

$$E\cos^2\alpha > E_{sbe,i}. \qquad (27)$$

The latter corresponds to an ion's reflection or a target atom's sputtering. The cutoff energy of any species is chosen equal to the surface binding energy of this species in order to obtain reflection and sputtering yields correctly.

2.2.6 *Surface binding energies*

The surface binding energies determine the sputtering yields of the elements in the substrate. A method for obtaining the surface binding energies is described in the following.

In the case of a monocomponent substance A, its surface binding energy is given by

$$E_{sbe,A} = \Delta H_A \qquad (28)$$

where ΔH_A is the sublimation heat of the monocomponent substance A.

In the case of a compound ($A_m B_n$), as atoms A and B exist in a molecular form, any atom needs an energy larger than the surface binding energy of its monocomponent substance to escape from the surface. According to W. Eckstein et al.[5], the surface binding energies of atoms A and B are determined from

$$\begin{aligned} E_{sbe,A} &= \Delta H_f + \Delta H_A, \\ E_{sbe,B} &= \Delta H_f + \Delta H_B \end{aligned} \qquad (29)$$

where ΔH_f is the formation heat of compound $A_m B_n$, and ΔH_A or ΔH_B is the sublimation heat of pure substance A or B. When compounds and monocomponent substances exist together in a target substance, a numeric interpolation method is used to calculate the surface binding energies according to the composition.

2.2.7 *Substrate relaxation*

The composition of the substrate is changed as additional atoms and vacancies are generated inside the substrate after ion implantation. So local expansion or contraction may be caused inside the substrate in order to accommodate the change in the local composition. A schematic diagram of the substrate relaxation is shown in Fig.1. The substrate is initially divided into a number of thin slabs of equal thickness. The thickness of each slab is chosen close to the thickness of a monatomic layer (about 2~3Å) according to Möller [6,7]. The substrate relaxation is arranged to be performed after the implantation of ions with a given differential flux ΔD_{ion}. The computational method for the substrate relaxation is described in the following.

If the change of the number of atomic species j in slab i is represented as ΔC_{ij} for one ion bombardment, the new area density of the atoms of species j in that slab is given by

$$A_{ij}=f_{ij}n_i\Delta X_i+\Delta C_{ij}\Delta D_{ion} \tag{30}$$

where n_i is the atomic volume density of slab i, ΔX_i is the thickness of slab i., and f_{ij} is the fraction of species j in slab i and satisfied with $\sum_{j=1} f_{ij}=1$. Therefore, the thickness of slab i is adjusted according to

$$\Delta X_i=\sum_{j=1} A_{ij}n_{eff,j}^{-1} \tag{31}$$

where $n_{eff,j}$ is the effective atomic volume density, which may be set as the atomic density of the pure components, or chosen to fit the correct atomic density of a given compound.

The thickness of each slab during the simulation is limited between 0.5ΔX and 1.5ΔX where ΔX is the initial thickness of each thin slab. When the thickness of each slab goes out of this range, that slab will be combined with its next slab or be split into two thin slabs.

2.2.8 Approach for the residual gas mixed into the growing film

In some special cases, residual gas in the vacuum chamber may affect the composition of the film formed during ion beam mixing. In the case when an easily oxidized substance is used as an evaporated substance, the oxygen of the residual gas seems to be deposited at the substrate surface as well as the evaporated substance. The experimental result given below has demonstrated this phenomenon. The reason for it is explained as follows.

According to gas molecular thermodynamics, the flux of molecules through a unit area per unit time is represented as

$$A=\frac{1}{4}n\bar{v}=\frac{p}{\sqrt{2\pi mkT}} \tag{32}$$

where n is the atomic density of the residual gas, $\bar{\upsilon}$ is the average speed of gas molecules, P is the pressure of residual gas, m is the mass of one molecule, k is Boltzmann's constant (1.3807x10-23), and T is the Kelvin temperature of the gas. In the case of the vacuum pressure $P=2\times10^{-6}$Torr and the temperature T=300K, the amount of oxygen atoms through a unit area per unit time is about 7.2x10^{14} atoms/cm^2 according to formula (32), providing that half of the residual gas is assumed as oxygen gas. On the other hand, if pure aluminum is chosen as the evaporated substance and its deposition rate is set in the range of 4~12Å/s, the ratio of oxygen and aluminum atoms arriving at the surface may vary from 0.1 to 0.3. Therefore, aluminum may be partly oxidized on the deposited layer by the oxygen of the residual gas in experiments.

In order to simulate the effect of oxygen mixing into the film during ion beam mixing, oxygen was assumed to deposit on the substrate surface simultaneously with aluminum at a given atomic ratio of O/Al in the present paper. So this oxygen deposition can be treated in a similar way to aluminum deposition in the computer simulation program.

2.3 Computer simulation program

With the use of the model described above, a computer simulation program for thin film formation during ion beam mixing has been made in Fortran 77 language. The flow chart of the program is shown in **Fig.5**.

As shown in (**a**), necessary data including ion energy, ion incident angle, the ratio of the evaporated atom-to-ion flux, and the relative material constants are entered. The substrate is divided into a number of thin slabs of equal thickness in the direction normal to the substrate surface. N is defined by $N = D/\Delta D$ where D and ΔD are the given total flux and differential flux of ions and evaporated atoms, respectively. A variable *Counter* is used to count the number of the program's executing a loop, and its initial value is set to 1. After the above preparation, the flow enters a loop which will be run N times repeatedly to simulate thin film formation. The evaporated atoms with the differential flux of ΔD_{atom} are first deposited on the substrate surface. The movement of 1000 incident ions and the recoiled atoms caused by these ions' implantation is simulated by the Monte Carlo Method in order to obtain statistical results such as the sputtering yields and the distribution of the implanted ions and atomic relocations. The flow chart for

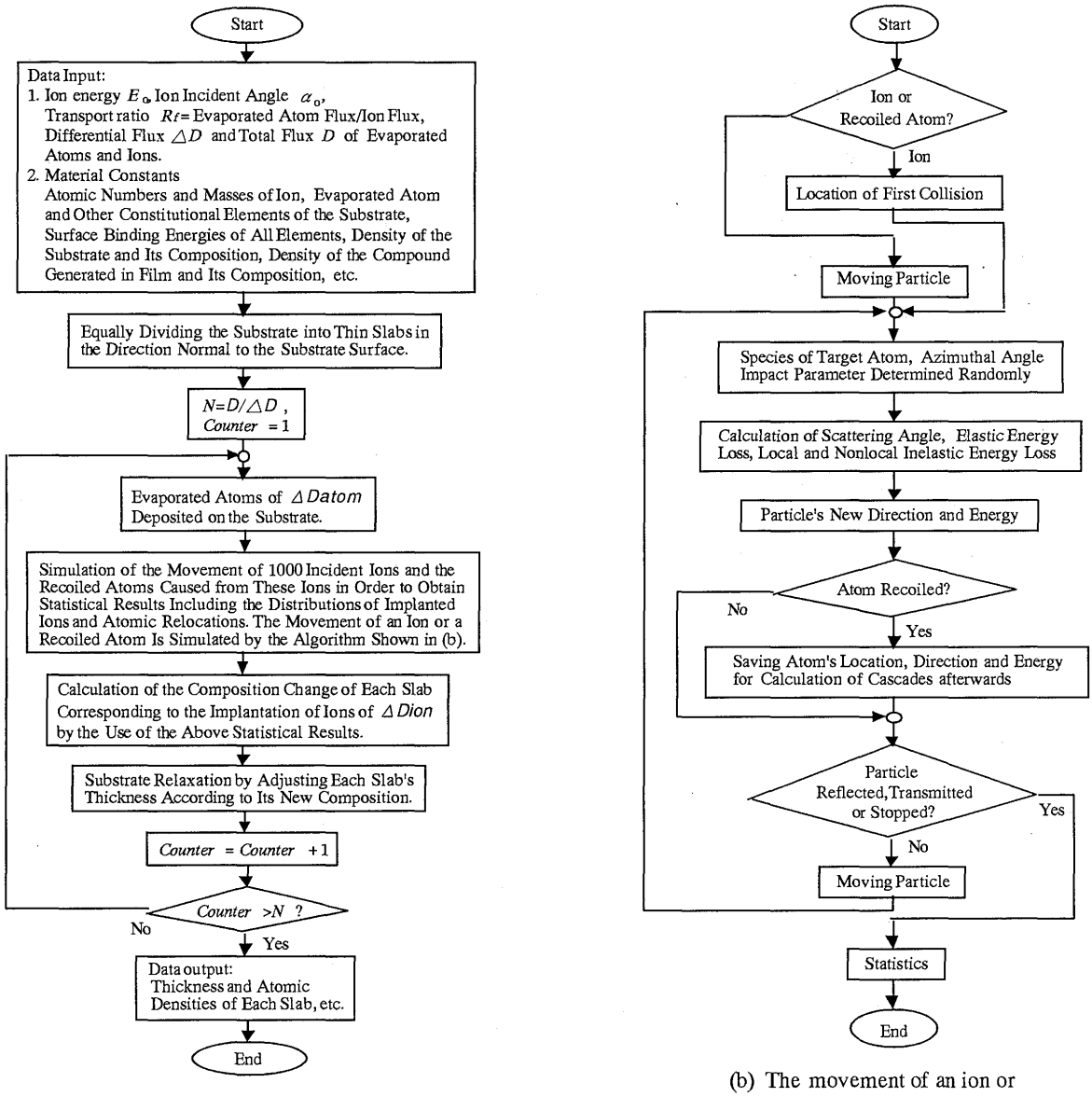

(a) Thin film formation.

(b) The movement of an ion or a recoiled atom in solid.

Fig.5 Flow chart for the simulation of thin film formation during ion beam mixing.

the simulation of the movement of a particle(ion or recoiled atom) is shown in **(b)**, in which an incident ion or a recoiled atom undergoes sequential binary elastic collisions until it is satisfied by stopping conditions described in *2.2.5* . For the implantation of ions with the differential flux ΔD_{ion}, the change of the composition in each slab is calculated by the use of the above statistical results. After evaporated atom deposition and ion implantation, the thickness of each slab is adjusted according to the change of the composition. At the end of the flow, data including the thickness and all atomic densities of each slab are generated.

3. Results and discussions

The computer simulations were performed for AlN film formation on a silica substrate at N^+ ion energies of 0.25, 0.5, 1.0 and 1.5keV and Al/N transport ratios of 0.5, 1.0, 1.5 and 2.0. The main input parameters were given as follows. The silica substrate was divided into a number of thin slabs with the same thickness of 2.5Å. The surface binding energies of Al, N, Si and O were chosen 3.36, 3.30, 14.14 and 9.44eV respectively according to equations (28) and (29). The differential flux of aluminum atoms and nitrogen ions was set $2.0\text{x}10^{13}$ atoms·cm^{-2}. On the other hand, all of the films were prepared experimentally under the conditions of room temperature, a vacuum pressure below $2.0\text{x}10^{-6}$ Torr, a fixed ion current density of 0.4mA/cm^2 and aluminum deposition rates of 4~12Å/s.

At a fixed Al/N transport ratio of 1.0, the composition-depth profiles obtained from the computer

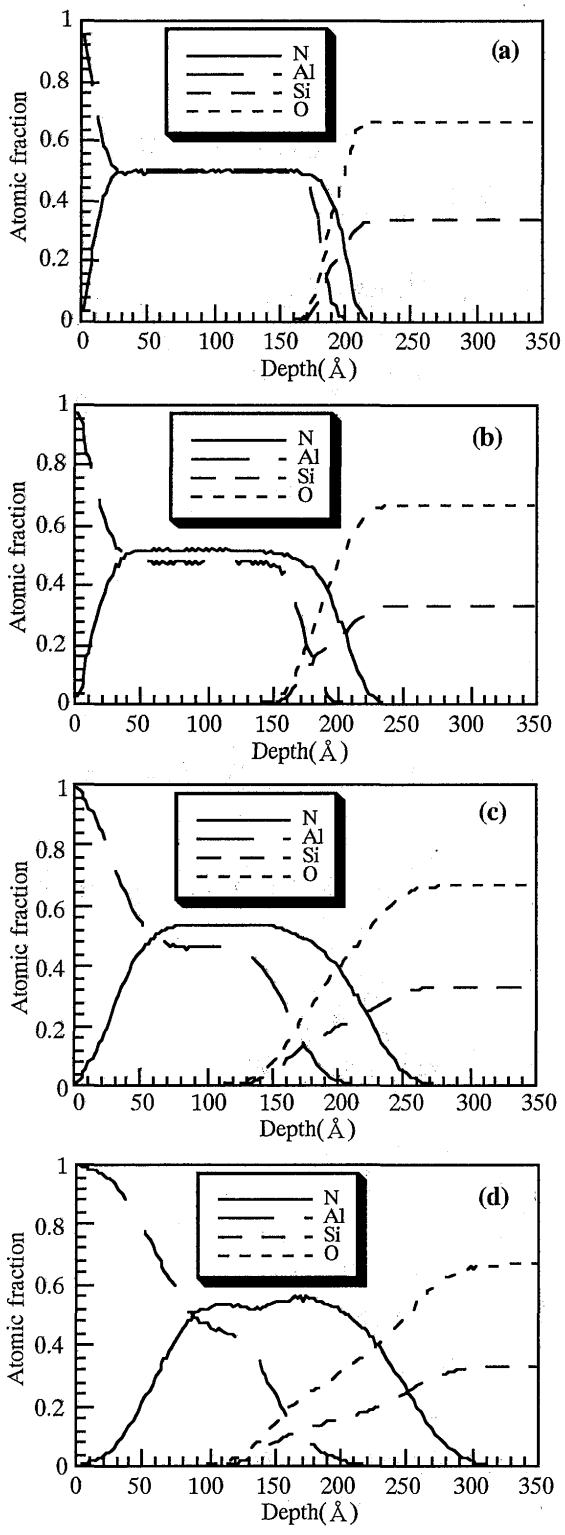

Fig.6 Composition-depth profiles obtained from the computer simulations at the same Al/N transport ratios of 1.0 and Al flux of 10^{17} atoms/cm^2 and different N^+ ion energies of 0.25(a), 0.5(b), 1.0(c) and 1.5keV(d).

simulations are shown in **Fig.6**. It is found that thin films are composed of three layers, i.e., the surface layer enriched with aluminum, the bulk layer with a constant composition(Al and N) and the mixing layer between the

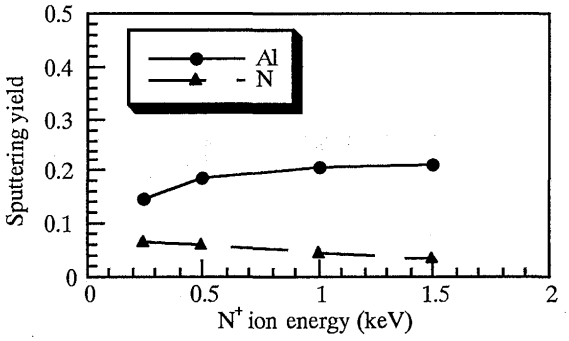

Fig.7 Sputtering yields of aluminum and nitrog depending on nitrogen ion energy.

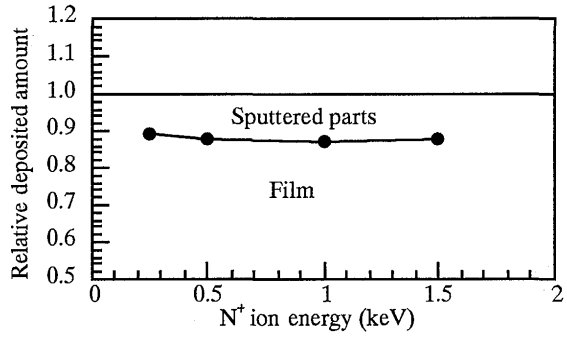

Fig.8 Relationship between the amount of aluminum and nitrogen deposited in the film and the nitrogen ion energy.

bulk layer and the substrate. Nitrogen always appears deeper inside the substrate than aluminum, and aluminum is always enriched in the surface. This is obviously due to the higher energy of incident ions compared with that of evaporated aluminum atoms. It is also noticed that both the surface layer and the mixing layer become broadened as the ion energy increases. This results from an increase in the ion range and straggle. Thealuminum concentration in the bulk layer decreases with an increase of ion energy. This is mainly due to an increase in aluminum sputtering yields.

The sputtering yields of Al and N corresponding to Fig.6 is shown in **Fig.7**. With an increase in the ion energy, the Al sputtering yield increases, but the N sputtering yield decreases. The reason for this difference is the decrease of nitrogen content in the surface layer, which has been shown in Fig.6. By subtracting the sputtered amount, the amount of Al and N deposited in the film can be found. **Fig.8** shows the relationship between the amount of deposited Al and N and the nitrogen ion energy. The deposited amount decreases little as the ion energy increases.

It is well known that the properties of a thin film are greatly dependant on the composition of the bulk layer, so it is of interest to investigate the effects of ion beam mixing conditions on the composition of the bulk layer by means of the computer simulation. **Fig.9** shows the

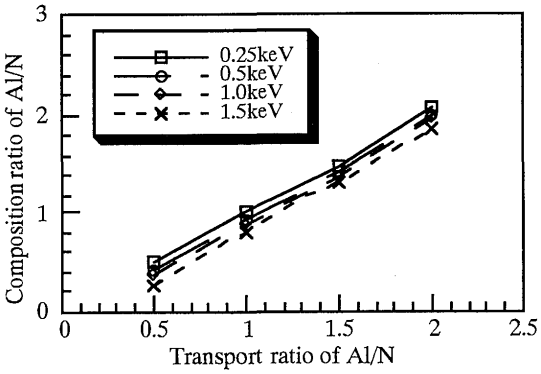

Fig.9 Effects of Al/N transport ratio and nitrogen ion energy on the composition of AlN bulk film.

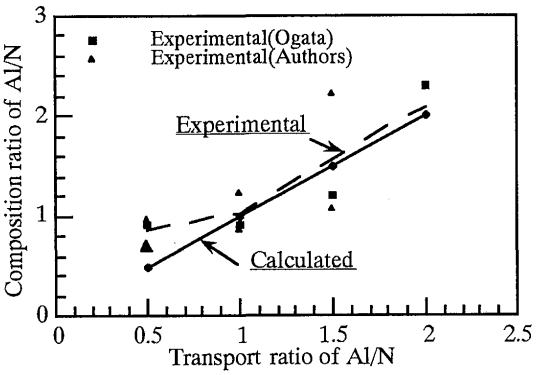

Fig.10 The comparison between experimental and calculated results of the composition of AlN bulk films under the condition of 0.25keV ion energy.

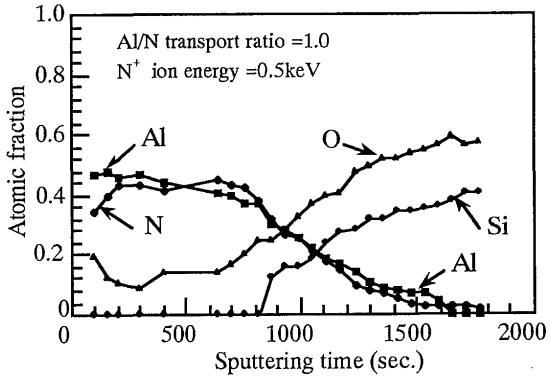

Fig.11 The composition-depth profile of an AlN film obtained from AES measurement.

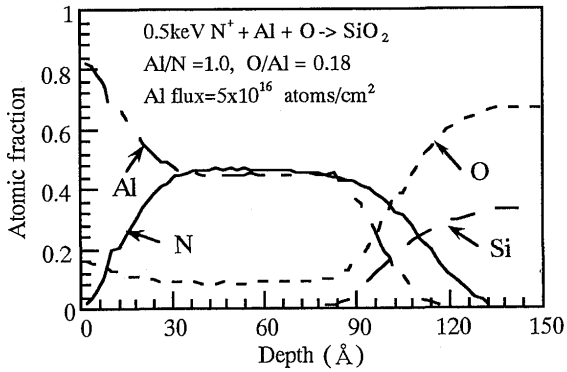

Fig.12 The calculated result of a composition profile by taking account of oxygen mixing into the film 0.18 O/Al ratio was used in computer simulation.

relationship between the composition and the Al/N transport ratio at different nitrogen ion energies. The Al/N composition ratio is nearly proportional to the Al/N transport ratio at the same ion energy. It is close to the Al/N transport ratio at the lower ion energy and decreases at the higher ion energy.

Several experimental results obtained by Ogata [12] and the authors have been compared with the computer simulations in **Fig.10**. A good agreement is found in the case of an Al/N transport ratio larger than or close to unity(stoichiometric Al/N composition ratio of AlN compound), and a large discrepancy exists in the case of an Al/N transport ratio much less than unity. It follows that the pure collision model is suitable for the case of the Al/N transport ratio larger than or close to unity. On the other hand, when the Al/N transport ratio is less than unity, an ion-induced superfluous nitrogen release becomes effective besides pure collisional effects. However, the mechanisms are still unknown.

AES measurements have been used to obtain the composition-depth profiles of AlN films in order to make a comparison between the experimental results and calculated ones. One of the experimental results is shown in **Fig.11**, in which the film was prepared at a nitrogen ion energy of 0.5keV and an Al/N transport ratio of 1.0. Besides oxygen mixed into the film, the composition-depth profile is also found to be composed of three layers the same as those in Fig.6 where oxygen was not considered to be mixed into the film. The oxygen concentration in the surface is near to 0.2, and much more than in the bulk region which is almost a constant. The oxygen content of the film is derived from the residual gas in the vacuum. The explanation for this oxygen mixing into the film has been given previously. **Fig.12** shows the composition-depth profile simulated at the same Al/N transport ratio and nitrogen ion energy as those in Fig.11, and an O/Al deposition ratio of 0.18. By comparing Fig.12 with Fig.11, a good agreement is found, except for the distribution of aluminum and nitrogen near to the substrate. This is believed to result from the previous deposition of evaporated aluminum before the ion beam mixing experiment. The authors have already verified experimentally this previous deposition of aluminum.

4. Conclusions

A computational model based on the BCA has been

described in detail. It has been demonstrated to be effective in the simulation of the formation of aluminum nitride films during ion beam mixing at a transport ratio of Al/N larger than or close to the stoichiometric ratio of the AlN compound, i.e., the composition of the bulk film is mainly determined by pure collisional effects. At a lower transport ratio of Al/N, the additional ion-induced superfluous nitrogen release must be incorporated into the present model in order to obtain correct results.

Concerning the effect of residual gas on the formation of the films, a new approach has been added into the present model, and proved to be an effective method to produce more reasonable calculated results.

References

1) G. Carter, I. V. Katardjiev and M. J. Nobes, Vacuum, 39(1989)571.
2) G. K. Hubler, C. A. Carsella and E. P. Donovan etc., Nucl. Instrum. Methods B, 46(1990)384.
3) J. P. Biersack and L. G. Haggmark, Nucl. Instrum. Methods, 174(1980)257.
4) J. P. Biersack and W. Echstein, Appl. Phys., A34(1984) 73.
5) W. Eckstein and J. P. Biersack, Appl. Phys. A, 37(1985) 95.
6) W. Möller and W. Eckstein, Nucl. Instrum. Methods B, 2(1984)814.
7) W. Möller, W. Eckstein and J. P. Biersack, Computer Physics Communications, 51(1988)355.
8) W. Möller, Thin Solid Films, 228(1993)319.
9) C. Nender, S. Berg and J. P. Biersack, Thin Solid Films, 193-194(1990)13.
10) W. Z. Li, F. Z. Cui, Y. Liao and H. D. Li, Vacuum, 40(1990)289.
11) D. Bouchier and W. Möller, Surf. Coat. Technol., 45 (1991)73.
12) K. Ogata, Y. Andoh and E. Kamijo, Nucl. Instrum. Methods B, 39(1989)178.
13) J. M. E. Harper, J. J. Cuomo and H. T. G. Hentzell, J. Appl. Phys., 58(1)(1985)550.
14) H. T. G. Hentzell, J. M. E. Harper and J. J. Cuomo, J. Appl. Phys., 58(1)(1985)556.
15) S. Kiyama, H. Hhirono and Y. Domoto etc., J. Jpn. Precision Eng. Soci., 60(7)(1994)1029.
16) W.D. Wilson, L.G. Haggmark and J.P. Biersack, Phys. Rev. B, 15(1977)2458.
17) J. Lindhard and M. Scharff, Phys. Rev., 124(1961)128.
18) O. S. Oen and M. T. Robinson, Nucl. Instrum. Methods, 132(1976)647.